Influence of diameter and annealing on the electrical and thermoelectric properties of electrodeposited $Bi_{0.89}Sb_{0.11}$ crossed nanowires

Cite as: Appl. Phys. Lett. **129**, 103903 (2026); doi: 10.1063/5.0349868
Submitted: 26 June 2026 · Accepted: 20 August 2026 ·
Published Online: 10 September 2026

Alexandru Carabogdan,[1,2] Tristan da Câmara Santa Clara Gomes,[2,3] Pascal Van Velthem,[2] Etienne Ferain,[2,4] Flavio Abreu Araujo,[2] Luc Piraux,[2,a)] and Vlad-Andrei Antohe[1,2,a)]

AFFILIATIONS

[1]Research and Development Center for Materials and Electronic and Optoelectronic Devices (MDEO), Faculty of Physics, University of Bucharest, Atomiştilor Street 405, 077125 Măgurele, Ilfov, Romania
[2]Institute of Condensed Matter and Nanosciences (ICMN), Université catholique de Louvain (UCLouvain), Place Croix du Sud 1, 1348 Louvain-la-Neuve, Belgium
[3]Instituto de Engenharia de Sistemas E Computadores – Microsistemas e Nanotecnologias (INESC MN), Rua Alves Redol 9, 1000-029 Lisbon, Portugal
[4]it4ip S.A., Avenue Jean-Etienne Lenoir 1, 1348 Louvain-la-Neuve, Belgium

[a)]**Authors to whom correspondence should be addressed:** luc.piraux@uclouvain.be and vlad.antohe@fizica.unibuc.ro

ABSTRACT

Interconnected networks of $Bi_{0.89}Sb_{0.11}$ crossed nanowires (CNWs) with controlled diameters were fabricated by electrodeposition within track-etched polyimide (PI) membranes, following a single irradiation step from multiple angles, by fine-tuning the density and pore diameter. These PI membranes exhibit excellent thermal resistance, allowing annealing at temperatures close to the melting point of the bismuth–antimony (Bi–Sb) alloy. For $Bi_{0.89}Sb_{0.11}$ CNWs with a diameter of 200 nm annealed at 285 °C, a significant increase in the Seebeck coefficient is observed, with values identical to those of the bulk alloy for temperatures between 170 and 320 K. Furthermore, a significant magneto-thermoelectric effect is observed at relatively low magnetic fields, which until now had only been reported in Bi–Sb alloy single crystals. The thermopower decreases with the reduction in nanowire diameter, as does the mobility of charge carriers. The temperature variations in electrical resistance and Hall coefficient are consistent with those of *n*-type semiconductors with narrow bandgap. These results are promising for obtaining flexible thermoelectric films for the direct conversion of wasted heat into electrical power.

Lightweight and flexible thermoelectric materials capable of directly converting thermal energy into electricity are attracting increasing interest for wearable electronics.[1–8] Among the various flexible thermoelectric systems, networks of interconnected nanowires electrodeposited in cross-porous polymer membranes are particularly promising because their architecture, dimensions, and composition can be readily tailored.[9–14] A key advantage of crossed nanowires (CNWs) embedded in polymer membranes is their ability to harvest thermal energy both in-plane and perpendicular to the nanocomposite film.[11,15] Moreover, their three-dimensional (3D) architecture enables transverse thermoelectric effects, as recently demonstrated by Nernst measurements on interconnected bismuth (Bi) nanowires.[12]

Bulk bismuth–antimony (Bi–Sb) alloys, long recognized for applications near and below room temperature,[16–18] have recently regained interest due to a marked enhancement in thermoelectric performance under weak magnetic fields achievable with permanent magnets.[19] The thermoelectric performance of a material is quantified by the dimensionless figure of merit, $ZT = S^2T/\rho\kappa$, where S is the Seebeck coefficient, ρ the electrical resistivity, κ the thermal conductivity, and T the absolute temperature. Although enhanced ZT values in high-quality Bi–Sb alloy single crystals under weak magnetic fields were previously reported,[20–22] recent measurements on high charge carrier mobility $Bi_{0.88}Sb_{0.12}$ single crystals yielded ZT values two to three times higher than in the zero field.[19] Consequently, record performance below room temperature was achieved, reaching $ZT = 1.7 \pm 0.2$ between 160 and 220 K for magnetic fields less than 1 T.[19] Since the figure of merit is proportional to the square of the Seebeck coefficient, this enhancement primarily originates from a giant magneto-Seebeck effect.

Electrochemical growth of Bi–Sb nanowire arrays typically yields properties inferior to bulk materials,[13,23,24] largely due to the use of track-etched polycarbonate membranes that preclude high-temperature post-annealing, a key step for optimizing thermoelectric performance.[25] In this work, we investigate the effects of annealing and diameter on the thermoelectric and magneto-transport properties of $Bi_{0.89}Sb_{0.11}$ CNWs, a composition corresponding to the maximum figure of merit.[26,27] These 3D nanostructures are fabricated by direct electrodeposition within high-temperature-resistant polyimide (PI) membranes featuring a 3D nanochannel network.

Track-etched PI membranes with interconnected pores of controlled diameter were fabricated using a single irradiation step with an energetic xenon (Xe) ion beam. As shown in Fig. 1(a), a roller placed in front of the beam guided the 25-μm-thick PI film, defining the track angular distribution ($\pm 35°$), while the film speed and beam intensity controlled the track density (5×10^8–10^{10} cm^{-2}). The tracks were converted into pores by selective chemical etching in aqueous sodium hypochlorite (NaOCl),[28] yielding pore diameters of $d = 50$, 80, and 200 nm at a constant porosity of 20%. Finally, a ≈ 15 nm chromium (Cr) adhesion layer and a ~ 2 μm copper (Cu) film were deposited *in situ* by electron-beam evaporation on one side of the templates

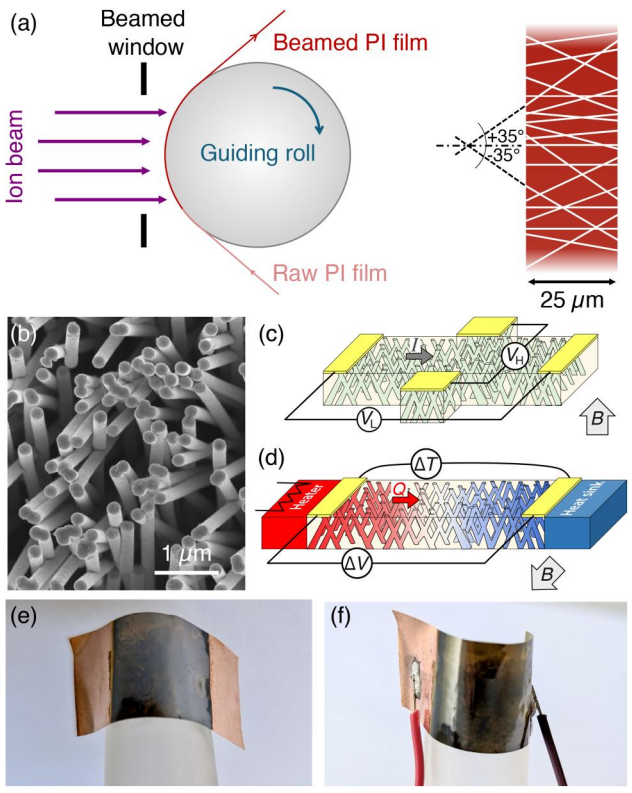

FIG. 1. (a) Schematic of the fabrication process for track-etched PI membranes with crossed cylindrical nanopores. (b) SEM image showing CNWs with a diameter of 200 nm. Design of the experimental setup configurations for Hall coefficient (c) and thermoelectric power (d) measurements. The direction of the magnetic field is indicated in each case. (e) and (f) Photographs illustrating the flexibility of the nanocomposite film based on CNWs and the soldering of connecting wires on the Cu electrodes.

to serve as cathode for subsequent electrodeposition (ECD) of the $Bi_{0.89}Sb_{0.11}$ alloy.

The $Bi_{0.89}Sb_{0.11}$ ECD process was reported elsewhere.[13] Briefly, a pulsed chronoamperometric deposition at ambient temperature ensured uniform filling of the PI templates, by alternating -0.32 V (for 10 ms) and -0.21 V (for 90 ms) vs a silver/silver chloride (Ag/AgCl) reference electrode. The Sb concentration of $\sim$11% was ensured by an optimal |Sb|/|Bi| molar ratio of 0.7 in the electrolyte. In order to achieve a similar degree of volumetric filling in the PI templates and to prevent the formation of macroscopic caps on the PI film surface, the electrodeposited charge was kept the same for all samples.

Figure 1(b) shows a scanning electron microscope (SEM) image of 200 nm diameter CNWs with a packing density of 20%, which are precise replicas of the original interconnected porous structure. The SEM micrograph was taken after the complete chemical dissolution of the PI template in a 1:1 mixture containing 1 M NaOH (sodium hydroxide) and NaOCl (6%–14% chlorine) at 70 °C for about 3 h. It should be noted that this method of synthesizing CNWs, which requires only a single irradiation step of the polymer film, is greatly simplified compared to previous work on 3D nanowires within polycarbonate membranes produced through successive irradiation steps at various angles.[9,29–33] Representative close-up SEM micrographs of the CNWs for the investigated diameters are also shown in Fig. S1 of the supplementary material.

Subsequently, the PI-$Bi_{0.89}Sb_{0.11}$ CNW composites were thermally annealed at 285 °C for 1 min under nitrogen (N_2) atmosphere, heated with a ramp of 10 °C/min and cooled at a similar rate. Notably, the annealing temperature was chosen near the alloy's melting point, which sensitively depends on the Sb content according to the corresponding phase diagram.[17,34] Owing to PI's superior thermal stability, with a glass transition temperature of approximately 400 °C[35] (significantly higher than that of the polycarbonate, of $\sim$150 °C,[36] and well above the melting point of Bi-rich Bi–Sb alloys), the nanocomposite and 3D CNWs architecture remained intact during annealing.

Elemental characterization of the $Bi_{0.89}Sb_{0.11}$ CNWs was performed after the complete dissolution of the PI template by energy-dispersive x-ray (EDX) analysis. X-ray diffraction (XRD) was carried out in a Bragg–Brentano configuration using a Bruker D8 Advance diffractometer operating with Cu K_α radiation, over an angular range (2θ) of 20°–75°. Phase identification was made using the American Mineralogist Crystal Structure Database (AMCSD). Prior to the XRD measurements, the Cu cathode layer from the back side of the PI templates was completely etched away galvanostatically at 0.5 A cm^{-2}, in a commercial Cu electrolyte.[12,13]

Electrical and thermoelectric measurements were performed after partial removal of the Cu cathode and cutting the samples into the desired geometries [Figs. 1(c) and 1(d)]. A Hall bar of about 1 cm long [Fig. 1(c)] was used for resistance, magnetoresistance, and Hall effect measurements between 15 and 300 K, with current injected through the remaining Cu cathode and silver (Ag) paint contacts, while taking advantage of the high degree of nanowire network interconnectivity, as recently demonstrated.[12,13] The magnetic field was applied perpendicular to the PI-CNWs nanocomposite films and varied between ± 0.8 T. Thermopower measurements were carried out between 50 and 320 K under vacuum using the setup shown in

Fig. 1(d).[12,13] An in-plane thermal gradient was generated by a resistive heater, while the thermovoltage and temperature difference were measured using Chromel-P leads and a type-E differential thermocouple, respectively. The magneto-Seebeck effect was studied by applying a magnetic field of up to 1 T, applied in the plane of the PI-CNW film, as shown in Fig. 1(d). The porous PI matrix provides flexibility and high thermal stability, enabling direct soldering of wires onto the metal electrodes [Figs. 1(e) and 1(f)].

Figure 2(a) shows the EDX spectra of $Bi_{0.89}Sb_{0.11}$ CNWs, revealing exclusively the constituent elements, i.e., Bi and Sb, with no detectable impurity and contaminant signals in the electrodeposited samples. Furthermore, the inset provides a quantitative elemental analysis, demonstrating that the Sb atomic content in the alloy is approximately 11%.

The XRD patterns of $Bi_{0.89}Sb_{0.11}$ CNWs with various diameters are presented in Fig. 2(b) for the as-prepared samples and in Fig. 2(c) for the samples annealed at 285 °C for 1 min. The patterns of the as-deposited samples [Fig. 2(b)] reveal the formation of a polycrystalline Bi–Sb solid compound with no evidence of separate phase complexes, consistent with our previous report.[13] After annealing at 285 °C [Fig. 2(c)], dominant reflections from (110) planes are observed for all samples, suggesting the CNWs alignment near the binary–bisectrix plane of the rhombohedral crystal system. In addition, the annealed sample with 200 nm diameters [red pattern in Fig. 2(c)] exhibits also an increase in the intensity of (012) diffraction peak, suggesting a more relaxed crystal structure which resembles the behavior of bulk Bi–Sb where the (012) planes obliquely oriented relative to the trigonal axis are preferentially favored.[37] The observed enhancement suggests that annealing promotes recrystallization and strain relaxation in the 200 nm sample, leading to improved structural order. However, after annealing, the (012) peak decreases in intensity at smaller diameters, the trend being attributed to the increasing influence of geometric confinement as the diameter is reduced.

The temperature variation of the thermoelectric power of the as-prepared and annealed $Bi_{0.89}Sb_{0.11}$ CNWs 200 nm in diameter is shown in Fig. 3(a). For comparison, previously measured values of the thermopower of a bulk $Bi_{0.90}Sb_{0.10}$ alloy[38] and a $Bi_{0.90}Sb_{0.10}$ thin film[39] are also shown in the same temperature range investigated. It is found that annealing leads to a significant increase in the absolute values of the thermopower over the entire temperature range due to a more homogeneous distribution of Sb atoms in the CNWs. At room temperature, the thermopower (−90 μV/K) is approximately twice as high for samples annealed at 250 and 285 °C compared to the as-deposited sample, while at around $T = 150$ K, the increase reaches a factor of 6. The temperature dependence of the thermopower is also significantly altered by annealing, as shown in Fig. 3(a). Indeed, the thermopower of as-deposited $Bi_{0.89}Sb_{0.11}$ CNWs decreases continuously with cooling below $T = 320$ K, while for $Bi_{0.89}Sb_{0.11}$ CNWs annealed at 285 °C, the thermopower increases up to $T \approx 150$ K, reaching values as high as −110 μV/K, before decreasing at lower temperatures. As seen in Fig. 3(a), the thermopower for $Bi_{0.89}Sb_{0.11}$ CNWs annealed at 285 °C is identical to that of bulk alloy down to $T \approx 170$ K. However, at lower temperatures, significant differences appear, with the maximum thermopower in bulk alloys occurring at around $T = 50$ K.[17,38,40] In these narrow bandgap semiconductors, it is known that the decrease in the Seebeck coefficient following the increase in temperature is due to thermal excitation.[19] Overall, the

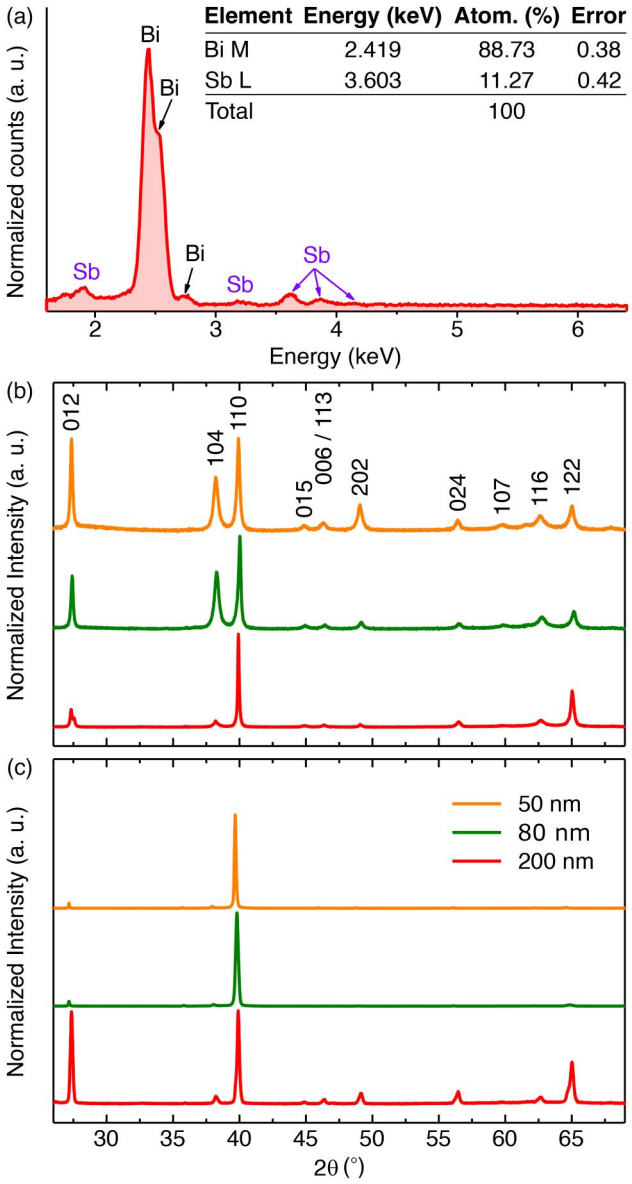

FIG. 2. (a) EDX analysis of the 3D interconnected $Bi_{0.89}Sb_{0.11}$ CNWs of 200 nm diameter. The inset represents corresponding quantitative calculations of the Bi and Sb atomic percentages, respectively. Normalized XRD patterns acquired on the $Bi_{0.89}Sb_{0.11}$ CNWs with diameters of 200 nm (red), 80 nm (olive), and 50 nm (cyan), before (b) and after (c) an annealing process at 285 °C for 1 min. Reference powder diffraction data of Bi (AMCSD 0012839) was used for peaks identification.

temperature variation in the thermopower of $Bi_{0.89}Sb_{0.11}$ CNWs resembles that of thin films of Bi–Sb alloys with equivalent composition.[39,41,42] In addition, the Seebeck coefficient of the annealed Bi–Sb CNWs shown in Fig. 3(a) is far above the values reported to date for parallel arrays of Bi–Sb nanowires prepared by ECD[23,24] and by injecting the molten alloy into the pores of anodic aluminum oxide templates,[43] whose values range from −30 to −50 μV/K at room

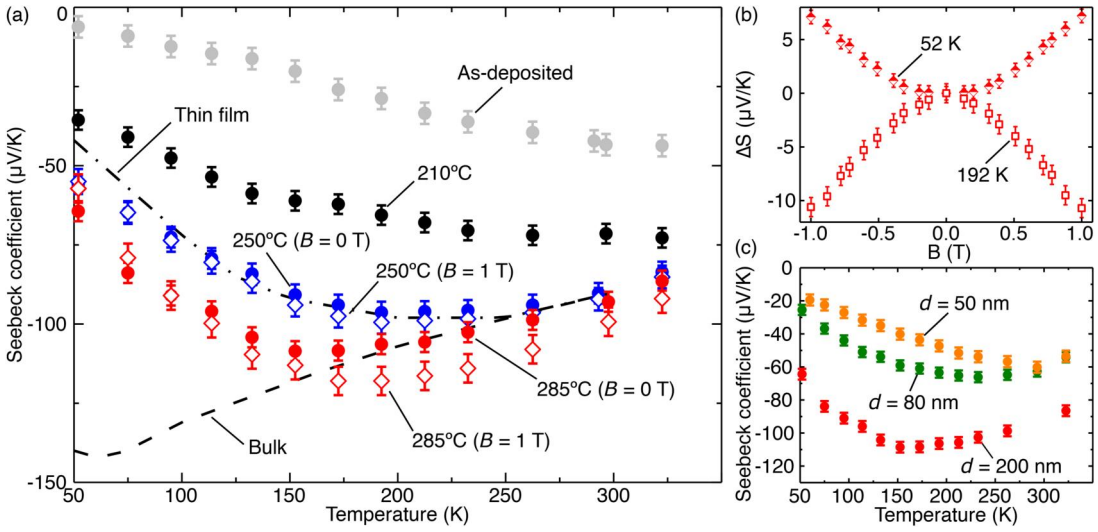

FIG. 3. (a) Temperature variation of the Seebeck coefficient of $Bi_{0.89}Sb_{0.11}$ CNWs with a diameter of 200 nm, as prepared and annealed at different temperatures, as indicated. The dashed lines show the data obtained on annealed $Bi_{0.90}Sb_{0.10}$ bulk alloy[38] and $Bi_{0.90}Sb_{0.10}$ thin film prepared by flash evaporation,[39] as indicated. (b) Magnetic field dependence of the thermopower of $Bi_{0.89}Sb_{0.11}$ CNWs annealed at 285 °C at two distinct temperatures, $T = 52$ K and $T = 192$ K. (c) Temperature dependence of the Seebeck coefficient of $Bi_{0.89}Sb_{0.11}$ CNWs annealed at 285 °C with diameters of 200, 80, and 50 nm.

temperature, demonstrating the importance of annealing at temperatures close to the melting point.

Measurements carried out on individual $Bi_{0.92}Sb_{0.08}$ nanowires with a diameter comparable to that in the present study, and annealed at 180 °C, yielded a resistivity of $5 \times 10^{-6}\,\Omega\,m$ at $T = 300$ K,[23] which is approximately three times higher than that of the bulk material. Furthermore, it is known that the thermal conductivity at room temperature of bulk Bi–Sb alloys of similar composition is mainly due to the electronic contribution (κ_E).[26] The Wiedemann–Franz law, $\kappa_E \rho = LT$, where L is the Lorenz number, is widely used to estimate κ_E. For non-degenerate semiconductors, it is known that a significant decrease in L occurs compared with the degenerate limit, where $L = 2.44 \times 10^{-8}\,V^2\,K^{-2}$. In a previous study, the Lorenz numbers of various thermoelectric materials based on measurements of Seebeck coefficients have been evaluated.[44] A rough estimate gives $L \sim 2 \times 10^{-8}\,V^2\,K^{-2}$ for Bi–Sb alloys. The figure of merit for bulk Bi–Sb alloys ($ZT \sim 0.3$ at $T = 300$ K) can be obtained equivalently from the expression $ZT = S^2/L(1 + \kappa_L/\kappa_E)$, with κ_L the lattice thermal conductivity, using the ratio $\kappa_L/\kappa_E \sim 0.2$ deduced from experimental data on electrical and thermal conductivities.[26] The lack of thermal conductivity measurements on Bi–Sb nanowires means that ZT cannot be determined. However, we can expect that the electronic and lattice components are likely to decrease in nanowires due to the increased scattering mechanisms of electrons and phonons. Therefore, since the Seebeck coefficients of the $Bi_{0.89}Sb_{0.11}$ CNWs annealed at 285 °C are identical to those of bulk materials at $T = 300$ K ($S \sim -90\,\mu V/K$), the figure of merit in annealed Bi–Sb CNWs should not differ significantly from that of bulk alloys near room temperature. However, this simple analysis warrants a more detailed theoretical study. Interestingly, $Bi_{0.89}Sb_{0.11}$ CNWs annealed at $T = 285$ °C also exhibit large magneto-thermopower effects with a maximum increase in $[S(B = 1\,T) - S(B = 0)]/S(B = 0) \approx 12\%$ for $180\,K < T < 230\,K$ while the effect is much less (~3%) for the sample annealed at $T = 250$ °C [see Fig. 3(a)]. No noticeable effect was observed for the sample annealed at $T = 210$ °C. To the best of our knowledge, such large magneto-Seebeck effects in Bi–Sb alloys have only been reported on single crystals, where the Seebeck coefficient increases by ~30%–60% under similar temperature and magnetic field conditions.[19,22] The magneto-thermopower signal $\Delta S = S(B) - S(B = 0)$ at $T = 192$ K for the $Bi_{0.89}Sb_{0.11}$ CNW sample annealed at $T = 285$ °C [Fig. 3(b)] shows a significant increase in the negative values of the Seebeck coefficient with the magnetic field, with no tendency toward saturation around the maximum field of 1 T, in agreement with previous results obtained on bulk alloys.[19,22] In light of these results and the above analysis, we can estimate an increase in the figure of merit of up to 25% in the temperature range 200–300 K under a magnetic field of 1 T. In contrast, the magneto-Seebeck effect changes sign for $T < 80$ K [see Fig. 3(a)], leading to a less negative Seebeck coefficient, as illustrated in Fig. 3(b) at $T = 52$ K. A similar change in the sign of ΔS at low temperatures has also been reported for bulk Bi–Sb alloys of the same composition.[19,22] The smaller magneto-Seebeck effects in $Bi_{0.89}Sb_{0.11}$ CNWs compared to single crystals can be attributed to lower carrier mobility and to prior single crystal measurements being performed along the trigonal direction, where mobility is maximal.[19] The large magneto-Seebeck response is theoretically linked to Dirac band dispersion characteristics of $Bi_{1-x}Sb_x$ topological materials coupled with ultra-high mobility of charge carriers.[19] Figure 3(c) compares the results obtained on 50 and 80 nm $Bi_{0.89}Sb_{0.11}$ CNWs annealed at 285 °C with the ones for 200 nm samples, showing a reduced Seebeck coefficient and a shift of its maximum toward higher temperatures with decreasing diameter, consistent with reduced mobility and diameter-induced modifications in the band structure characteristics of Bi–Sb nanowires.

The temperature dependence of the electrical resistance of the $Bi_{0.89}Sb_{0.11}$ CNWs (with $d = 200$, 80, and 50 nm) annealed at $T = 285$ °C is shown in Fig. 4(a). The data have been normalized to the resistance value at room temperature. All samples exhibit typical

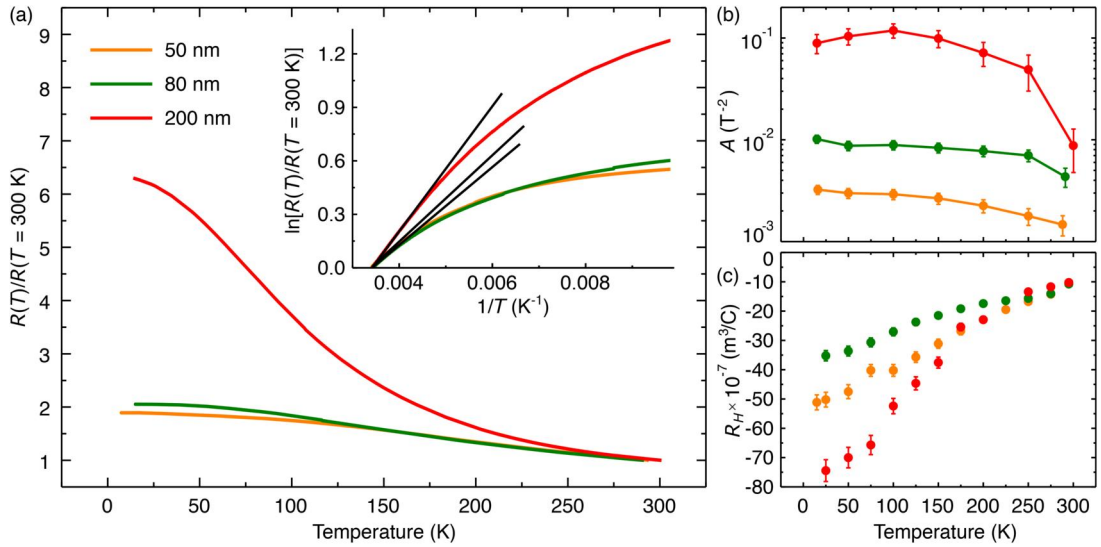

FIG. 4. Temperature dependence of the electrical resistance (a), amplitude of the magnetoresistance coefficient A (b) and Hall coefficient R_H (c) of $Bi_{0.89}Sb_{0.11}$ CNWs annealed at 285 °C with diameters of 200, 80, and 50 nm. The data in (a) are normalized to electrical resistance values obtained at room temperature. The inset in (a) shows the variation of the logarithm of the normalized resistance vs the inverse of temperature for all samples.

narrow bandgap semiconductor behavior, where the temperature dependence of carrier density dominates over the opposing temperature dependence of mobility. Similar temperature variations in electrical resistance have been reported in thin films and nanowires of Bi–Sb alloys.[13,37,39,40,43,45] In the high-temperature range, the electrical resistance shows an exponential temperature dependence, i.e., $R(T) \approx \exp(\epsilon_g/2kT)$, with ϵ_g being the bandgap.[46] From the curves in the inset of Fig. 4(a), where the logarithm of the normalized resistance is plotted as a function of $1/T$, the bandgap ϵ_g was estimated to be ∼50, 36, and 30 meV, for $d = 200$, 80, and 50 nm, respectively. Those values agree with the values previously reported for nanostructured Bi–Sb alloys, thin films, and nanowires.[13,39,42,45,47] Low-field magnetoresistance measurements were performed on the annealed $Bi_{0.89}Sb_{0.11}$ CNWs with $d = 200$, 80, and 50 nm at different temperatures between $T = 25$ K and room temperature. All samples show a classical quadratic variation of magnetoresistance with magnetic field, i.e., $\mathrm{MR} = [R(B) - R(B = 0)]/R(B = 0) = AB^2$ (see the supplementary material, Fig. S2). Figure 4(b) shows the temperature dependence of the A coefficient for various samples. The A coefficient has units of electron mobility squared, hence its decrease with decreasing diameter is attributed to enhanced surface and grain-boundary scattering contributions to the electrical resistance. Hall effect measurements on $Bi_{0.89}Sb_{0.11}$ CNWs [Fig. 4(c)] show that the Hall coefficient R_H is virtually identical at room temperature across all diameters, while its reduction with decreasing temperature is stronger for the 200 nm sample, consistent with its larger temperature-dependent resistance variation [Fig. 4(a)]. By considering the $Bi_{0.89}Sb_{0.11}$ alloy as one-type carrier system, the electron carrier concentration (n) can be estimated from the simple relationship $R_H = 1/ne$. For the CNWs with $d = 200$ nm, this gives $n \approx 6 \times 10^{18}$ cm^{-3} at room temperature and $n \approx 8 \times 10^{17}$ cm^{-3} at $T = 25$ K. For the 80 and 50 nm samples, the carrier density is somewhat larger in the low-temperature range. While carrier concentrations at room temperature are very similar to those found in bulk Bi–Sb alloys of same composition, values at low temperatures are significantly higher in nanowires.[38,42,48] Furthermore, it has been theoretically predicted that in Bi–Sb single-crystal nanowires with diameters in the range 20–50 nm, quantum confinement may alter the electrical and thermoelectric properties.[49] Such effects are not observed in our study, due to the larger diameters and polycrystalline nature of the electrodeposited Bi–Sb CNWs.

We demonstrate the fabrication of high-temperature-resistant cross-porous track-etched PI membranes using a simplified process involving a single irradiation step. Annealing at temperatures close to the melting point of 3D networks of electrodeposited $Bi_{0.89}Sb_{0.11}$ CNWs with a diameter of 200 nm leads to Seebeck coefficients close to those of bulk alloys over a wide temperature range near and below room temperature, reaching values of $-110\ \mu$V/K around $T = 150$ K. Measurements carried out under magnetic fields up to 1 T reveal large magneto-Seebeck effects, leading to a significant increase in the negative thermopower for samples annealed at $T = 285$ °C. The Seebeck coefficient and charge carrier mobility both decrease with reducing CNWs diameter. The Hall effect measurements carried out on these $Bi_{0.89}Sb_{0.11}$ CNWs are consistent with the expected behavior of narrow bandgap n-type semiconductors. These results mark a crucial step toward the development of flexible thermoelectric devices based on 3D nanowire networks. In future work, we intend to apply the same synthesis approach to produce Bi–Te and Bi–Sb–Te alloys, which are expected to yield p-type flexible films with ZT values greater than 1.[7,8]

See the supplementary material for the SEM micrographs of the $Bi_{0.89}Sb_{0.11}$ CNWs of various diameters, as well as for the corresponding magnetoresistance data acquired at different temperatures for all samples.

Financial support was provided by the Belgian Fund for Scientific Research (F.R.S.–FNRS). A. C. would like to thank

Wallonie-Bruxelles International (WBI) for its support. F. A. A. receives support as a Research Associate of the F.R.S.–FNRS. Authors would like to thank François Devred for his help with the XRD measurements. Financial support was provided by the European Union. Views and opinions expressed are, however, those of the authors only and do not necessarily reflect those of the European Union or the European Research Executive Agency (REA). Neither the European Union nor the granting authority can be held responsible for them. T. d. C. S. C. G. is an ERA fellow.

AUTHOR DECLARATIONS

Conflict of Interest

The authors have no conflicts to disclose.

Author Contributions

Alexandru Carabogdan: Data curation (equal); Formal analysis (equal); Investigation (equal); Visualization (equal); Writing – original draft (equal); Writing – review & editing (equal). **Tristan da Câmara Santa Clara Gomes:** Data curation (equal); Software (equal); Visualization (equal). **Pascal Van Velthem:** Formal analysis (equal); Investigation (equal); Methodology (equal). **Etienne Ferain:** Investigation (equal); Resources (equal); Visualization (equal). **Flavio Abreu Araujo:** Data curation (equal); Software (equal); Visualization (equal). **Luc Piraux:** Conceptualization (equal); Formal analysis (equal); Funding acquisition (equal); Investigation (equal); Methodology (equal); Project administration (equal); Resources (equal); Supervision (equal); Validation (equal); Visualization (equal); Writing – original draft (equal); Writing – review & editing (equal). **Vlad-Andrei Antohe:** Data curation (equal); Formal analysis (equal); Investigation (equal); Methodology (equal); Resources (equal); Supervision (equal); Validation (equal); Visualization (equal); Writing – original draft (equal); Writing – review & editing (equal).

DATA AVAILABILITY

The data that support the findings of this study are available from the corresponding authors upon reasonable request.

REFERENCES

[1]Y. Chen *et al.*, "Bendable *n*-type metallic nanocomposites with large thermoelectric power factor," Adv. Mater. **29**, 1604752 (2017).
[2]Y. Wang *et al.*, "Flexible thermoelectric materials and generators: Challenges and innovations," Adv. Mater. **31**, 1807916 (2019).
[3]Z. Fan, Y. Zhang, L. Pan, J. Ouyang, and Q. Zhang, "Recent developments in flexible thermoelectrics: From materials to devices," Renewable Sustainable Energy Rev. **137**, 110448 (2021).
[4]L. Zhang, X. L. Shi, Y. L. Yang, and Z. G. Chen, "Flexible thermoelectric materials and devices: From materials to applications," Mater. Today **46**, 62–108 (2021).
[5]H. Zhou, X. Zhang, Z. Luo, X. Wei, and H. Deng, "Flexible thermoelectric materials and devices for sensing applications," Mater. Horiz. **13**, 194–218 (2026).
[6]K. Manojkumar *et al.*, "Flexible thermoelectrics for wearable electronics: Trends and benchmarks in solid-state and ionic materials, textile architectures, interface engineering, and device performance," Adv. Electron. Mater. **12**, e00396 (2026).
[7]Z. H. Zheng *et al.*, "Harvesting waste heat with flexible Bi_2Te_3 thermoelectric thin film," Nat. Sustainable **6**, 180–191 (2022).
[8]Z. H. Zheng *et al.*, "Ultrahigh thermoelectric properties of *p*-type $Bi_xSb_{2-x}Te_3$ thin films with exceptional flexibility for wearable energy harvesting," Carbon Energy **6**, e541 (2024).
[9]T. da Câmara Santa Clara Gomes, F. Abreu Araujo, and L. Piraux, "Making flexible spin caloritronic devices with interconnected nanowire networks," Sci. Adv. **5**, eaav2782 (2019).
[10]F. Abreu Araujo, T. da Câmara Santa Clara Gomes, and L. Piraux, "Magnetic control of flexible thermoelectric devices based on macroscopic 3D interconnected nanowire networks," Adv. Electron. Mater. **5**, 1800819 (2019).
[11]T. da Câmara Santa Clara Gomes, N. Marchal, F. Abreu Araujo, and L. Piraux, "Flexible thermoelectric films based on interconnected magnetic nanowire networks," J. Phys. D **55**, 223001 (2022).
[12]L. Piraux *et al.*, "Polycrystalline bismuth nanowire networks for flexible longitudinal and transverse thermoelectrics," Nanoscale **15**, 13708–13717 (2023).
[13]L. Piraux *et al.*, "Improved electrical and thermoelectric properties of electrodeposited $Bi_{1-x}Sb_x$ nanowire networks by thermal annealing," Nanoscale Adv. **7**, 124–132 (2025).
[14]T. da Câmara Santa Clara Gomes, N. Marchal, J. de la Torre Medina, F. Abreu Araujo, and L. Piraux, "22 - Magneto-thermoelectric effects in magnetic nanowire networks," In *Magnetic Nano- and Microwires*, 3rd ed., Woodhead Publishing Series in Electronic and Optical Materials, edited by M. Vázquez (Woodhead Publishing, 2026), pp. 657–678.
[15]M. F. P. Wagner *et al.*, "Effects of size reduction on the electrical transport properties of 3D Bi nanowire networks," Adv. Electron. Mater. **7**, 2001069 (2021).
[16]G. S. Nolas, J. Sharp, and H. J. Goldsmid, *Thermoelectrics: Basic Principles and New Materials Developments*, 1st ed., Springer Series in Materials Science (Springer, Berlin, Heidelberg, 2001).
[17]B. Lenoir, H. Scherrer, and T. Caillat, "Chapter 4 An overview of recent developments for BiSb alloys," in *Recent Trends in Thermoelectric Materials Research I*, Semiconductors and Semimetals, edited by T. M. Tritt (Elsevier, 2001), Vol. 69, pp. 101–137.
[18]J. P. Heremans and H. Jin, "Thermoelectric and spin-caloritronic coolers: From basics to recent developments," Proc. SPIE **9765**, 976507 (2016).
[19]Y. Pan *et al.*, "A magneto-thermoelectric with a high figure of merit in topological insulator $Bi_{88}Sb_{12}$," Nat. Mater. **24**, 76–82 (2025).
[20]R. Wolfe and G. E. Smith, "Effects of a magnetic field on the thermoelectric properties of a bismuth-antimony alloy," Appl. Phys. Lett. **1**, 5–7 (1962).
[21]W. M. Yim and A. Amith, "Bi–Sb alloys for magneto-thermoelectric and thermomagnetic cooling," Solid-State Electron. **15**, 1141–1165 (1972).
[22]M. Murata, A. Yamamoto, Y. Hasegawa, and T. Komine, "Magnetic-field dependence of thermoelectric properties of sintered $Bi_{90}Sb_{10}$ alloy," J. Electron. Mater. **45**, 1875–1885 (2016).
[23]S. Heiderich *et al.*, "Magnetotransport and thermopower of single $Bi_{0.92}Sb_{0.08}$ nanowires," Phys. Status Solidi RRL **7**, 898–902 (2013).
[24]M. Cassinelli *et al.*, "Influence of surface states and size effects on the Seebeck coefficient and electrical resistance of $Bi_{1-x}Sb_x$ nanowire arrays," Nanoscale **9**, 3169–3179 (2017).
[25]M. P. Siegal, A. L. Lima-Sharma, P. A. Sharma, and C. Rochford, "Correlating thermoelectric properties with microstructure in $Bi_{0.8}Sb_{0.2}$ thin films," Appl. Phys. Lett. **110**, 141905 (2017).
[26]B. Lenoir, M. Cassart, J. P. Michenaud, H. Scherrer, and S. Scherrer, "Transport properties of Bi-rich Bi–Sb alloys," J. Phys. Chem. Solids **57**, 89–99 (1996).
[27]H. Jin and J. P. Heremans, "Optimization of the figure of merit in $Bi_{100-x}Sb_x/Al_2O_3$ nanocomposites," Phys. Rev. Mater. **2**, 115401 (2018).
[28]E. Ferain and R. Legras, "Track-etch templates designed for micro- and nanofabrication," Nucl. Instrum. Methods Phys. Res., Sect. B **208**, 115–122 (2003).
[29]E. Araujo *et al.*, "Artificially modified magnetic anisotropy in interconnected nanowire networks," Nanoscale **7**, 1485–1490 (2015).
[30]L. Piraux, V. A. Antohe, E. Ferain, and D. Lahem, "Self-supported three-dimensionally interconnected polypyrrole nanotubes and nanowires for highly sensitive chemiresistive gas sensing," RSC Adv. **6**, 21808–21813 (2016).
[31]A. Vlad *et al.*, "Three-dimensional interconnected Ni_{core}–NiO_{shell} nanowire networks for lithium microbattery architectures," J. Mater. Chem. A **4**, 1603–1607 (2016).
[32]J. O. Omale *et al.*, "Three-dimensional microsupercapacitors based on interdigitated patterns of interconnected nanowire networks," Energy Storage Mater. **21**, 77–84 (2019).

[33]J. O. Omale, P. Van Velthem, V. A. Antohe, A. Vlad, and L. Piraux, "Effects of electrolyte additives and nanowire diameter on the electrochemical performance of lithium-ion battery anodes based on interconnected nickel-tin nanowire networks," Energy Tech. **9**, 2100062 (2021).
[34]H. Okamoto, "Bi–Sb (Bismuth–Antimony)," J. Phase Equilib. Diffus. **33**, 493–494 (2012).
[35]Z. Dai *et al.*, "Prediction of glass transition temperatures of polyimide for thermal safety from molecular structures," J. Therm. Anal. Calorim. **151**, 4651 (2026).
[36]C. Rochford, D. L. Medlin, K. J. Erickson, and M. P. Siegal, "Controlling compositional homogeneity and crystalline orientation in $Bi_{0.8}Sb_{0.2}$ thermoelectric thin films," APL Mater. **3**, 126106 (2015).
[37]K. Malik *et al.*, "Sb concentration dependent structural and resistive properties of polycrystalline Bi–Sb alloys," J. Appl. Phys. **112**, 083706 (2012).
[38]H. Kitagawa, H. Noguchi, T. Kiyabu, M. Itoh, and Y. Noda, "Thermoelectric properties of Bi–Sb semiconducting alloys prepared by quenching and annealing," J. Phys. Chem. Solids **65**, 1223–1227 (2004).
[39]E. Osmic *et al.*, "Thermopower and magnetotransport properties of $Bi_{100-x}Sb_x$ topological insulator thin films prepared by flash evaporation," J. Phys. Chem. Solids **167**, 110734 (2022).
[40]R. Martin-Lopez *et al.*, "Thermoelectric properties of mechanically alloyed Bi–Sb alloys," Appl. Phys. A **68**, 597–602 (1999).
[41]I. Vurgaftman *et al.*, "Thermoelectric and magnetotransport properties of $Bi_{1-x}Sb_x$ thin films and Bi/CdTe superlattices," J. Phys.: Condens. Matter **11**, 5157 (1999).
[42]S. Cho, A. DiVenere, G. K. Wong, J. B. Ketterson, and J. R. Meyer, "Thermoelectric transport properties of n-doped and p-doped $Bi_{0.91}Sb_{0.09}$ alloy thin films," J. Appl. Phys. **85**, 3655–3660 (1999).
[43]Y. M. Lin, O. Rabin, S. B. Cronin, J. Y. Ying, and M. S. Dresselhaus, "Semimetal-semiconductor transition in $Bi_{1-x}Sb_x$ alloy nanowires and their thermoelectric properties," Appl. Phys. Lett. **81**, 2403–2405 (2002).
[44]H. S. Kim, Z. M. Gibbs, Y. Tang, H. Wang, and G. J. Snyder, "Characterization of Lorenz number with Seebeck coefficient measurement," APL Mater. **3**, 041506 (2015).
[45]C. H. Will *et al.*, "Effect of nanostructuring on the band structure and the galvanomagnetic properties in $Bi_{1-x}Sb_x$ alloys," J. Appl. Phys. **114**, 193707 (2013).
[46]A. L. Jain, "Temperature dependence of the electrical properties of bismuth–antimony alloys," Phys. Rev. **114**, 1518–1528 (1959).
[47]S. Cho, A. DiVenere, G. K. Wong, J. B. Ketterson, and J. R. Meyer, "Transport properties of $Bi_{1-x}Sb_x$ alloy thin films grown on CdTe(111)*B*," Phys. Rev. B **59**, 10691–10696 (1999).
[48]K. Vandaele, B. He, P. Van Der Voort, K. De Buysser, and J. P. Heremans, "Wet-chemical synthesis of enhanced-thermopower $Bi_{1-x}Sb_x$ nanowire composites for solid-state active cooling of electronics," Phys. Rev. Appl. **9**, 024020 (2018).
[49]S. Tang and M. S. Dresselhaus, "Electronic phases, band gaps, and band overlaps of bismuth antimony nanowires," Phys. Rev. B **89**, 045424 (2014).